Supporting Information

A rheological study of the association and dynamics of MUC5AC gels

Caroline E. Wagner [†1], Bradley S. Turner [‡2], Michael Rubinstein [§3], Gareth H. McKinley [¶1], and Katharina Ribbeck [*2]

[1]Department of Mechanical Engineering, Massachusetts Institute of Technology, Cambridge, MA 02139

[2]Department of Biological Engineering, Massachusetts Institute of Technology, Cambridge, MA 02139

[3]Department of Chemistry, University of North Carolina, Chapel Hill, North Carolina 27599-3290

S1 Rheological response of MUC5AC gels purified with CsCl gradient centrifugation at pH2 and pH7

Smith and Lamont have shown that non-mucin proteins can be nearly completely removed from the mucin purified from bovine gallbladder mucus using CsCl gradient centrifugation[1]. As such, in order to assess the impact of non-mucin proteins on the rheology of MUC5AC gels, we have repeated the microrheological and macrorheological measurements at pH2 and pH7 using mucin purified with CsCl gradient centrifugation. These results are presented in Figure S1 below. For convenience in this discussion, we refer to mucins that have been prepared using CsCl gradient centrifugation as CsCl-MUC5AC, and those that have not as N-CsCl-MUC5AC.

[†]cewagner@mit.edu
[‡]bsturner@mit.edu
[§]mr@unc.edu
[¶]gareth@mit.edu
[*]ribbeck@mit.edu, Author to whom all correspondence should be addressed

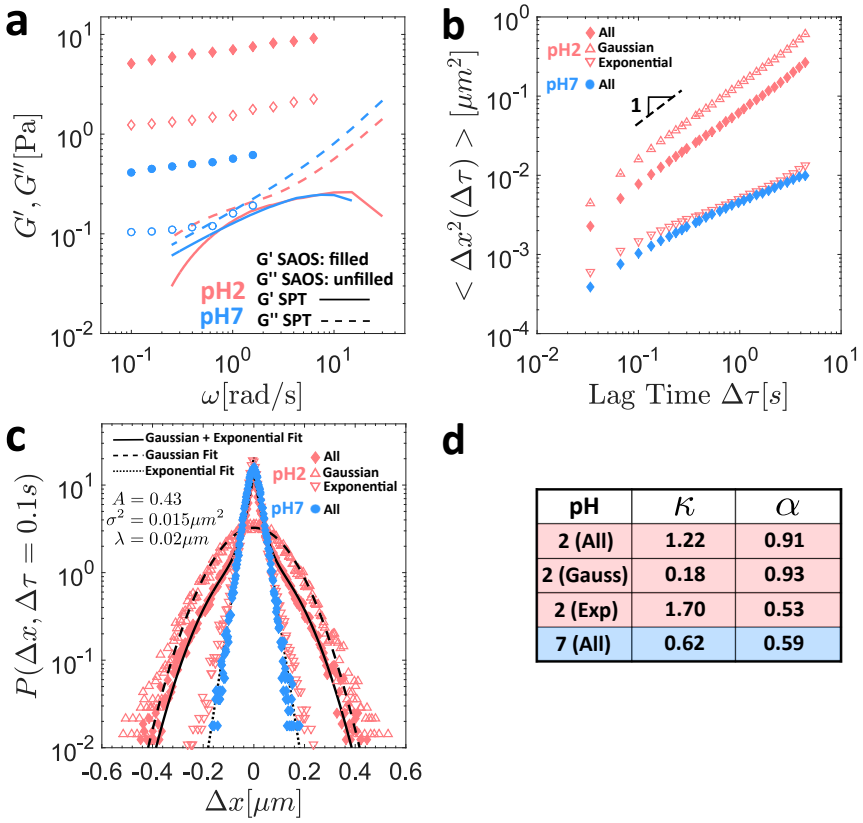

pH	κ	α
2 (All)	1.22	0.91
2 (Gauss)	0.18	0.93
2 (Exp)	1.70	0.53
7 (All)	0.62	0.59

Figure S1: Rheological response of 1 wt % MUC5AC gels purified with CsCl gradient centrifugation at pH2 and pH7. In (a) the linear viscoelastic response measured macroscopically (symbols) as well as the predicted moduli from the MSD data (lines) are presented. The aggregate MSD of all particle trajectories was used to calculate the viscoelastic moduli at pH7, whereas only the MSD of the exponential particle population was used at pH2. In (b) the MSD of the aggregate particle population as a function of the lag time is shown at pH2 and pH7. In addition, the individual MSDs corresponding to just the Gaussian and just the exponential particle populations are shown for the pH2 gel. In (c) the van Hove distributions for the same particle populations presented in (b) are shown, and in (d) a summary of the key microrheological parameters corresponding to the data presented in (a), (b), and (c) is provided.

Macroscopically, as with the N-CsCl-MUC5AC, the CsCl-MUC5AC gels are substantially stiffer at pH2 than at pH7, as seen in Figure S1a. However, the CsCl-MUC5AC gels are stiffer at *both* pHs compared to equivalent preparations of N-CsCl-MUC5AC. In particular, at pH7 G' and G'' of the N-CsCl-MUC5AC gels are very similar (Figure 2a of the main text) which is suggestive of a critical gel, while the CsCl-MUC5AC gels exhibit significantly more elastic, solid-like behaviour ($G' > G''$) under identical preparation conditions. The MSD of the same carboxylated, 1 µm particles used in the main text is larger at pH2 than at pH7 in the CsCl-MUC5AC gels as seen in Figure S1b, as was the case for the N-CsCl-MUC5AC gels (Figure 4a of the main text). This appears to again be associated with a large degree of heterogeneity within the pH2 gels, as measured by the non-Gaussian parameter κ which is significantly larger at pH2 than at pH7. Interestingly, however, κ is higher at pH7 for the CsCl-MUC5AC gels than for the same

preparation of N-CsCl-MUC5AC gels presented in the main text; in fact, the step size distribution at pH7 in Figure S1c is closer to an exponential than a Gaussian. The non-Gaussian parameter κ and the anomalous diffusion exponent α for the Gaussian (pH2), exponential (pH2) and aggregate (pH2, pH7) particle populations are presented in Figure S1d.

The increased stiffness of the CsCl mucin gels is consistent with CsCl-MUC5AC containing a higher percentage of the large, gel-forming MUC5AC mucins for an equivalent dry weight of purified mucin than N-CsCl-MUC5AC as a result of the removal of non-mucin proteins in this additional purification step. Further, we suspect that CsCl gradient centrifugation results in a mild denaturation of the MUC5AC mucins[2], and that in particular it may cause a partial unfolding of the hydrophobic domains of the molecules which are otherwise concealed at pH7 (see Section 3.1.1 of the main text). Under acidic conditions (pH2), these domains are believed to already be unfolded (a crucial step in the gelation process), and hence this may explain why greater differences between the CsCl-MUC5AC and N-CsCl-MUC5AC gels are seen at pH7 than at pH2. The higher degree of heterogeneity within the CsCl-MUC5AC gels at pH7 is also consistent with this idea of denaturation. Specifically, partial unfolding of the hydrophobic domains may promote a certain degree of the mesoscopic phase separation conjectured to exist at pH2, which would result in a higher degree of heterogeneity at pH7 than expected based on the response of the N-CsCl-MUC5AC gels at neutral pH.

To summarize then, CsCl gradient centrifugation is suspected to influence the purified mucin product in two ways: i) it increases the relative quantity of MUC5AC by removing non-mucin proteins, and ii) it may cause a mild denaturing of the MUC5AC by partially unfolding the globular hydrophobic domains. This results in both qualitative and quantitative differences in the microrheological and macrorheological measurements, and these differences are more pronounced at pH7. In particular, at neutral pH the CsCl-MUC5AC gels are more heterogeneous and are predominantly solid-like on the macroscopic scale over the entire frequency range probed, whereas the N-CsCl-MUC5AC solutions are homogeneous, critical gels. In order to assess the methods of network formation in MUC5AC gels for as close to the native state of the mucin molecules as possible, we choose to use N-CsCl-MUC5AC in the present study. Therefore, as a result of the omission of the additional CsCl gradient centrifugation step, it is possible that non-mucin proteins contribute to the rheological response of the gels. However, the lion's share of this rheological response is almost certainly still owed to the presence of the large mucin molecules[3].

S2 Strain sweep data for the MUC5AC gels

Strain sweep experiments were performed for every mucin preparation condition prior to SAOS measurements in order to determine the linear viscoelastic regime of each solution. These results are shown in Figure S2 for the varied pH (a), surfactant (b), and salt (c) preparations. The dashed lines denote the percent strain at which the corresponding SAOS measurements for each mucin solution presented in the main text were performed (Figures 2a, 2b, and 6a). The angular frequency at which each strain sweep experiment was performed is also indicated. For the softest gels in particular (such as those prepared at pH7 or at pH2 with 20 wt % surfactant), selecting the 'correct' or optimal conditions for performing these strain sweep experiments is ultimately a trade off between generating sufficient signal in torque and maintaining the raw phase angle as low as possible such that the inertia correction of the instrument is successful.

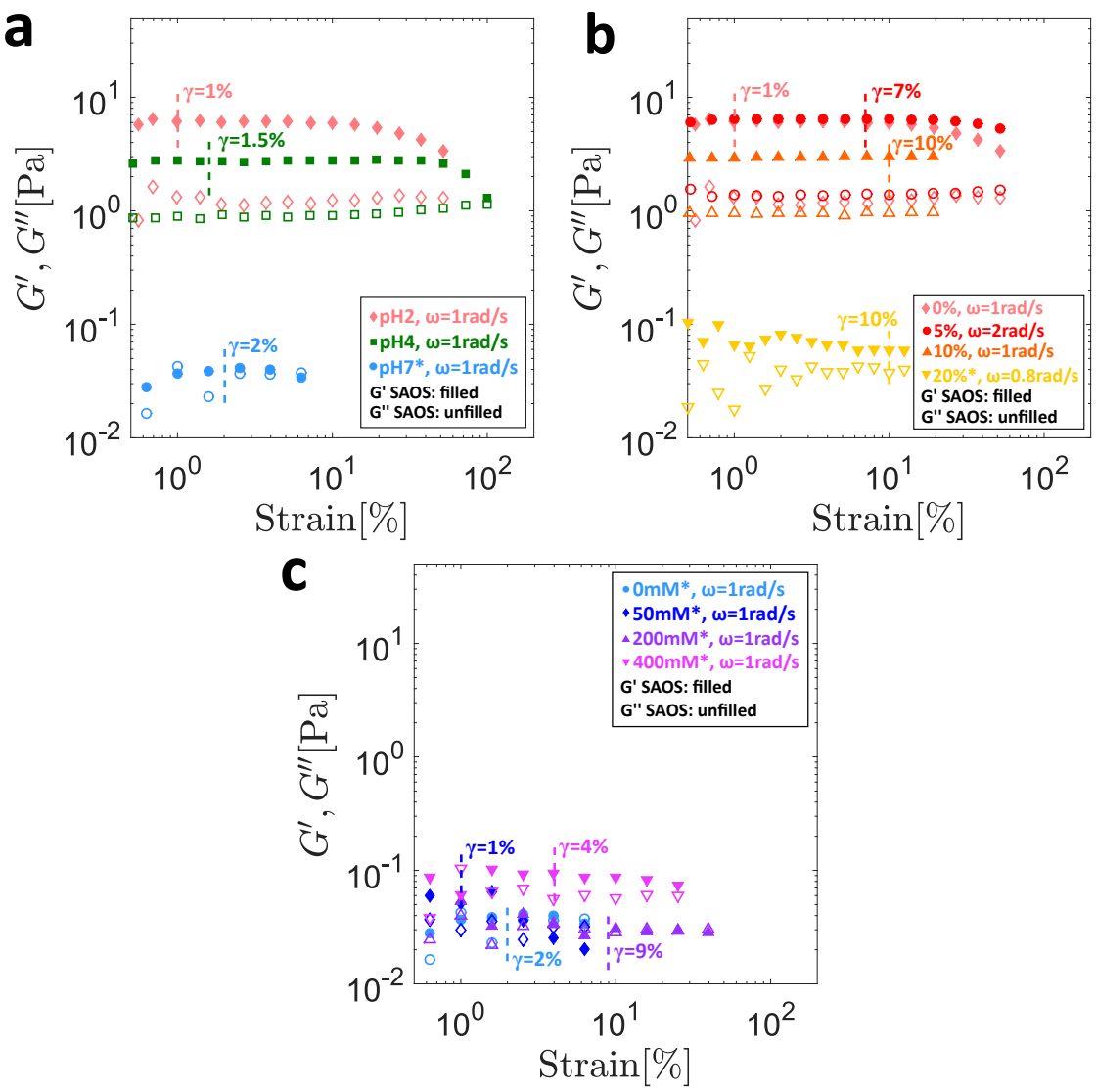

Figure S2: (a) Strain sweep experiments for 1 wt % purified MUC5AC mucin solutions as a function of (a) the pH; (b) the surfactant concentration; and (c) the salt concentration. The angular frequencies at which the experiments were performed are indicated, and the values of the strain at which the SAOS measurements reported in the main text (Figures 2a, 2b, and 6a) were performed are indicated with a dashed line. The asterisks denote experiments for which some or all of the reported strain sweep data points had associated raw phase angles $\delta_{\text{raw}} \geq 175°$.

S3 Additional mathematical details of the particle sorting procedure

For the sake of clarity, we present the details of the sorting procedure used in this study for the pH2 MUC5AC gel replicate with the greatest variance in MSD values between individual particle trajectories ($\text{var}(\overline{\Delta x_k^2(\Delta\tau)})$). We begin by following the method of Gao and Kilfoil[4] and fit a mixed probability distribution function to the van Hove distribution of all of the particles in a given experimental replicate at an early lag time of $\Delta\tau = 0.1\,\text{s}$ (see Figure 5a of the main text). However, unlike Gao and Kilfoil[4] who

consider combinations of Gaussian distributions, we define the mixed probability distribution function for the mucin gel system as the weighted sum of a Gaussian distribution and an exponential distribution, i.e.

$$P_{\text{fit}}(\Delta x, \Delta\tau) = \frac{A(\Delta\tau)}{\sqrt{2\pi\sigma^2}} \exp\left(-\frac{\Delta x^2}{2\sigma^2}\right) + \frac{(1 - A(\Delta\tau))}{2\lambda} \exp\left(-\frac{|\Delta x|}{\lambda}\right). \tag{S3.1}$$

The lag time dependent weights $0 \leq A(\Delta\tau) \leq 1$ and $(1 - A(\Delta\tau))$ signify the fraction of steps distributed normally and exponentially, respectively, and sum to unity for a normalized probability distribution.

In agreement with the previous observation of Valentine et al.[5], we find that the van Hove plot of each *individual* particle can be approximated as a normal Gaussian distribution even though the composite van Hove distribution accounting for the step sizes of *all* particles is clearly not Gaussian (solid pink symbols of Figure 5a in the main text). Thus, we next fit Gaussian distributions of the form

$$P_{\text{fit},i}(\Delta x, \Delta\tau) = \frac{1}{\sqrt{2\pi\sigma_i^2}} \exp\left(-\frac{\Delta x^2}{2\sigma_i^2}\right) \tag{S3.2}$$

to the step size distribution of each individual particle, obtaining an associated variance σ_i^2 for every fitted trajectory. In order to recover the overall probability distribution function P_{fit} defined in Equation (S3.1), the distributions of these individual variances σ_i^2 must satisfy

$$\int_0^\infty P_G(\sigma_i^2) P_{\text{fit},i} d\sigma_i^2 = \frac{A(\Delta\tau)}{\sqrt{2\pi\sigma^2}} \exp\left(-\frac{\Delta x^2}{2\sigma^2}\right) \tag{S3.3}$$

and

$$\int_0^\infty P_e(\sigma_i^2) P_{\text{fit},i} d\sigma_i^2 = \frac{(1 - A(\Delta\tau))}{2\lambda} \exp\left(-\frac{|\Delta x|}{\lambda}\right), \tag{S3.4}$$

where $P_G(\sigma_i^2)$ and $P_e(\sigma_i^2)$ are the distributions of the variances of the particles in the Gaussian and exponential subgroups, respectively, at each lag time $\Delta\tau$.

It is straightforward to show that Equation (S3.3) is satisfied for

$$P_G(\sigma_i^2) = A(\Delta\tau)\delta(\sigma_i^2 - \sigma^2), \tag{S3.5}$$

where δ is the Dirac delta function. For the exponential population, Chechkin et al.[6] have recently shown that when combined with a Gaussian, an exponential distribution of generalized diffusion coefficients $D_{\alpha,i}$ of the individual particle trajectories (or similarly an exponential distribution of their variances σ_i^2) results in the exponential distribution of step sizes defined in Equation (S3.4). Consequently, we take $P_e(\sigma_i^2)$ to be

$$P_e(\sigma_i^2) = \frac{(1 - A(\Delta\tau))}{2\lambda^2} \exp\left(-\frac{\sigma_i^2}{2\lambda^2}\right). \tag{S3.6}$$

To sort the K particles into the two subgroups, we select the $(1 - A) \times (K)$ particles whose variances σ_i^2 are best described by the distribution function in Equation (S3.6) as the exponential ones, and the remainder are taken to comprise the Gaussian population. In the case where a single particle population is observed after fitting the mixed distribution in Equation (S3.1) to the van Hove plot (i.e. $A = 0$ or $A = 1$), the trajectories of all particles for that experimental replicate are used in the calculation of the exponential or Gaussian statistics, respectively, as well as the aggregate population statistics for that gel condition.

The distributions of the variances for both of these populations as well as the aggregate one are shown in Figure S3, along with the unweighted predicted exponential distribution $P_e(\sigma_i^2)$ of the exponential group and the expected variance σ^2 of the Gaussian population. It is clear for this latter group that experimental noise results in a broader distribution for σ_i^2 than the predicted Dirac delta function ($P_G(\sigma_i^2)$ in Equation (S3.5)), although its peak is still closely approximated by σ^2.

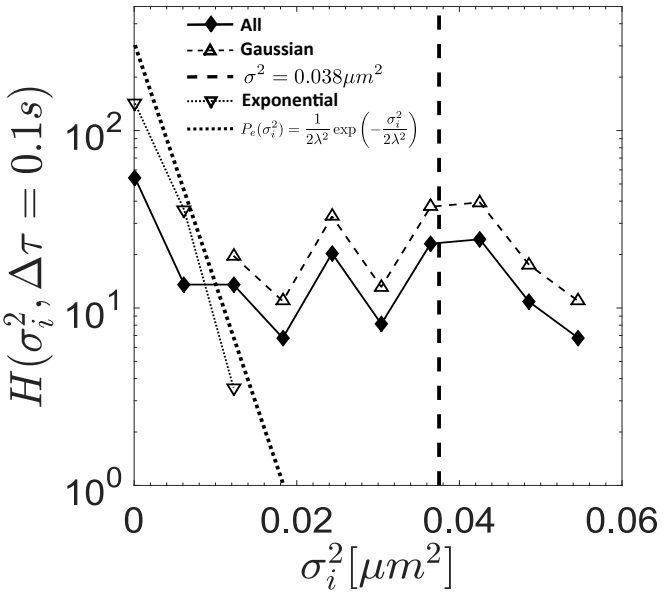

Figure S3: Distributions of the variances σ_i^2 of the individual particle trajectories are presented for the Gaussian (hollow triangles and a dashed line), exponential (hollow inverted triangles and a dotted line) and aggregate (filled diamonds and a solid line) populations, along with the predicted distribution $P_e(\sigma_i^2)$ (Equation (S3.6) and the thick dotted line) and a thick dashed line indicating the fitted value σ^2.

References

[1] Smith, B. F.; LaMont, J. T. *J. Biol. Chem.* **1984**, *259*, 12170–12177.

[2] Snary, D.; Allen, A.; Pain, R. H. *Biochem. J.* **1974**, *141*, 641–646.

[3] Bansil, R.; Turner, B. S. *Curr. Opin. Colloid Interface Sci.* **2006**, *11*, 164–170.

[4] Gao, Y.; Kilfoil, M. L. *Phys. Rev. Lett.* **2007**, *99*, 1–4.

[5] Valentine, M. T.; Kaplan, P. D.; Thota, D.; Crocker, J. C.; Gisler, T.; Prud'homme, R. K.; Beck, M.; Weitz, D. A.; Prudhomme, R.; Beck, M.; Weitz, D. A. *Phys. Rev. E* **2001**, *64*, 061506.

[6] Chechkin, A. V.; Seno, F.; Metzler, R.; Sokolov, I. M. *Phys. Rev. X* **2017**, *7*, 021002.